A New Active 3D Optical Proximity Sensor Array and Its Readout Circuit

Sheng-Chieh Huang, Wei-Hsuan Hsu, Paul C.-P. Chao, *Senior Member, IEEE*, and Che Hung Tsai

***Abstract*— A new 3-D proximity sensor panel (3-D touch panel) for a single object is proposed in this paper. The sensor panel consists of a photo detector (PD) array as active pixels, along with its optics design, a computation algorithm, and sensing circuitry to eliminate background lighting. This sensing panel system acts as a noncontact 3-D positioning sensor, which is able to sense spatial positions of the object without realistic touching to the panel. New active readout pixel circuits for the PDs are designed to efficiently convert PD-received light intensities to voltage signals. It offers high readout resolutions, larger output ranges, and lower noises, as compared with the conventional active pixel sensor (APS) with a 3T-structure (called 3T-APS). Toward success of the sensor, background light is eliminated by a specially designed sample and hold circuitry, whereas a computation algorithm for 3-D object detection is developed based on photometry. The circuit is fabricated by Taiwan Semiconductor Manufacturing Company 0.35-μm 2P4M 3.3 V mixed signal CMOS process. Sensing trials for a moving object are finally conducted. The sensor performance is validated and further illustrated by a Labview program. The sensing errors of a sphere object are successfully limited to 5% in percentages.**

***Index Terms*— Active pixel sensor (APS), photo detectors, photometry, 3D proximity sensor.**

I. Introduction

MOST of touch sensing products in the market nowadays are aimed for 2D sensing. Related touch panel technologies are developed in a fast pace and vastly used in the mobile devices and the video game products. Many of the ATMs, cell phones and the vending machines are equipped with touch panels. In recent years, there has been increasing interests in extending "touch-sensing" to "proximity-sensing," which has been developed for an extended time. The proximity technologies to date can be categorized into three different types: (14) capacitance proximity sensors [1]–[2], (2) inductance proximity sensors [3], and (3) optical proximity sensors [4]–[11]. Most of the afore-mentioned works are limited to detecting objects very close to the sensor panel. This study is the first to propose a 3D proximity sensing panel and its computation algorithm, which can be used to realize so-called 3D touch panels, 3D keyboards, or installed at the end effectors of robots [7]–[11] for sensing the distance and position of an object that may not be close to the touch panel. To this end, the proposed sensor panel in fact consists of arrays of light diode emitters (LEDs) and photo- detectors (PDs), where the PDs are the critical components of the entire system. It is known that a photo detector functions properly as it successfully transfers the photon to the current (photocurrents). A special readout circuit is designed herein for the PDs to transforms efficiently their output currents to voltage signals with noise reduced and output ranges enlarged. The readout circuits and the PDs constitute a so-called active pixel sensor (APS) array. Developed APS circuits are widely used to realize the function of converting the output currents of the PDs to voltage readings in wide ranges but low noises [12], [13]. Together with an array of LEDs, the PDs and APS array/circuits are successfully extended in this study to a 3D single-object sensing panel, as shown in Fig. 1.

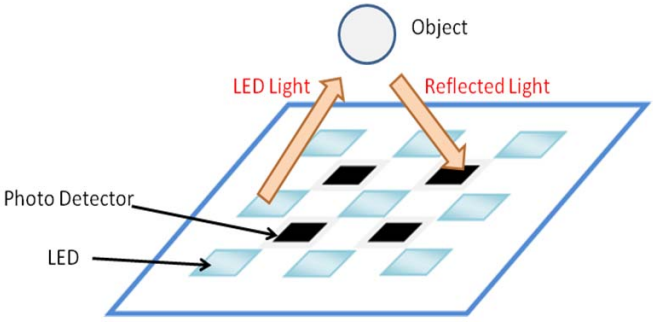

Fig. 1. The schematic of the proposed optical 3D single-object proximity sensing panel.

The proposed 3D optical proximity sensing panel system as shown in Fig. 1 is designed to be capable of detecting a single object in non-contact with the panel or even in a moderate distance to the panel. In this panel, the sensing components, i.e., photo-diodes (PDs), employed by this study are inorganic photo-gate devices fabricated by a standard CMOS technology [14], not the others like a-Si photodiode [15], since CMOS PDs enjoy benefits of low cost and high adaptability. As the 3D sensing panel in operations, the LEDs act as the light sources that emit light to the object. The reflected light from the object to sense is received by PDs. By acquiring the output voltage levels of the PDs and conducting the

Manuscript received January 22, 2014; accepted February 12, 2014. Date of publication February 19, 2014; date of current version May 22, 2014. This work was supported in part by the National Chip Implementation Center, National Science Council of Taiwan under Grant NSC 101-2623-E-009-006-D and in part by the UST-UCSD International Center of Excellence in Advanced Bio-Engineering through the Taiwan National Science Council I-RiCE Program under Grant NSC-101-2911-I-009-101. The associate editor coordinating the review of this paper and approving it for publication was Prof. Walter Lang.

The authors are with the Electrical Engineering Department, National Chiao Tung University, Hsinchu 300, Taiwan (e-mail: schuang@cn.nctu.edu.tw; shiwayshan0@hotmail.com; pchao@mail.nctu.edu.tw; xiaobudian.cht@gmail.com).

Color versions of one or more of the figures in this paper are available online at http://ieeexplore.ieee.org.

Digital Object Identifier 10.1109/JSEN.2014.2306846

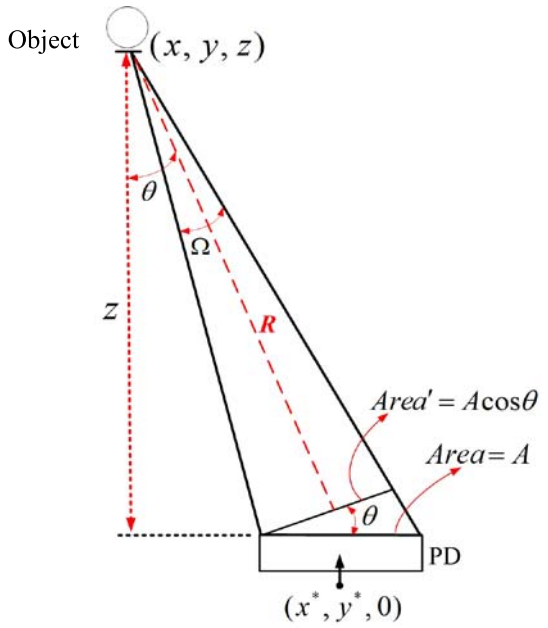

Fig. 2. The optics geometry between a PD surface and the object to detect.

computation based on the ensuing developed algorithm, the optical proximity sensor system is able to detect the position and distance of the target object. The computation algorithm is developed based on basic optics principles, where varied output voltage signals of multiple PDs are extracted to reversely estimate the 3D coordinates of the object to detect based on geometric optics and related power analysis. Note that different from conventional 2D capacitance or resistance touch panels, the proposed proximity sensor array owns the capability of sensing the distance of the object along the perpendicular axis of the panel surface.

II. Readout Computation Algorithms

The front part of the proposed 3D sensor system is a panel module composed of inter-placed PD and LED arrays. The object for sensing its 3D coordinates is assumed to be a general white color styrofoam ball. With the object offering a spherical surface to the sensor panel, according to the photometry [16], it can be assumed that the object is a Lambertian surface and the LED is also a Lambertian emitter. A simplified schematic showing the object and PD is depicted in Fig. 2, where (x, y, z) is the object coordinates, while $(x*, y*, 0)$ is the center coordinates of a PD surface plane placed at base surface z=0. With the above assumed conditions, the radiant flux detected by a single PD, as denoted by I_{PD}, is proportional to the projection of the PD surface on the plane normal to the centerline of the solid angle, i.e., "$cos\theta \times \Omega$," where θ is the angle between the PD surface and that perpendicular to the R-axis, while Ω is the solid angle from the target object to the sensor panel, which can be expressed by

$$\Omega = \frac{A \cdot \cos\theta}{R^2}, \tag{1}$$

where R is the distance between the object and the projected surface perpendicular to the R-axis, as denoted in Fig. 2, while A is the area of the PD. Thus, the LED irradiance on the PD, I_{PD}, is

$$I_{PD} = \alpha_0 \cdot \cos\theta \cdot \Omega = \frac{\alpha_0 \cdot A \cdot \cos^2\theta}{R^2}, \tag{2}$$

where α_0 is the assumed proportionality of the LED irradiance on the PD, I_{PD}, to the aforementioned "projected solid angle," "$cos\theta \times \Omega$." Substituting basic approximation of "$cos\theta \quad z/R$" to Eq. (2), one can obtain

$$I_{PD} = \alpha_0 \Omega \cos\theta \approx \frac{\alpha_0 A z^2}{R^4} = \frac{\alpha \cdot z^2}{[z^2 + (x - x^*)^2 + (y - y^*)^2]^2}, \tag{3}$$

where $\alpha = \alpha_0 A$ is a constant to be identified. On the other hand, the output voltage of the PD can then be expressed as

$$V_{out} = A_{amp} \cdot \frac{T}{C_{in}} \cdot I^*_{PD}, \tag{4}$$

where A_{amp} is the gain of the later-designed readout circuit. T is the discharge time of photodiodes as connected to the readout circuit. C_{in} is the parasitic capacitance at the negative end of photodiode. I^*_{PD} is the photocurrent, which is supposed to be proportional to the pre-defined PD-detected light intensity, I_{PD}. Substituting Eq. (3) into Eq. (4) yields

$$V_{out} = A_{amp} \cdot \frac{T}{C_{in}} \cdot \frac{\alpha^* \cdot z^2}{[z^2 + (x - x^*)^2 + (y - y^*)^2]^2}. \tag{5}$$

Since A_{amp}, T, C_{in} and α^* are constants, we can define

$$\beta \equiv A_{amp} \cdot \frac{T}{C_{in}} \cdot \alpha^*. \tag{6}$$

Substitution of Eq. (6) into Eq. (5) yields the output voltage of a PD as

$$V_{out} = \frac{\beta \cdot z^2}{[z^2 + (x - x^*)^2 + (y - y^*)^2]^2}. \tag{7}$$

Based on the above Eq. (7), the 3D coordinates of the object to detect can be predicted based on multiple voltage outputs of PDs in the developed 3D proximity array.

A 2×2 PD array as shown in Fig. 3 is considered to demonstrate development of the computation algorithm based on optics principles. As the PD array senses the object, the four PDs in the 2×2 PD array output four different voltage signals, abiding by Eq. (7). When the object approaches the sensor panel, the PDs and readout circuit would output larger voltage levels. The rear-end signal processing unit is designed to choose three largest voltage outputs from four PDs for the ensuing computation to predict the 3D coordinates of the object for maximum sensitivity and accuracy. According to Eq. (7), the output signals of the three PDs can be expressed as

$$V_1 = \frac{\beta z^2}{(z^2 + x^2 + y^2)^2}, \tag{8}$$

$$V_2 = \frac{\beta z^2}{(z^2 + x^2 + (d - y)^2)^2}, \tag{9}$$

$$V_3 = \frac{\beta z^2}{(z^2 + (d - x)^2 + y^2)^2}, \tag{10}$$

where d is the distance between adjacent PDs as defined in Fig. 3. Solving the above three highly nonlinear equations

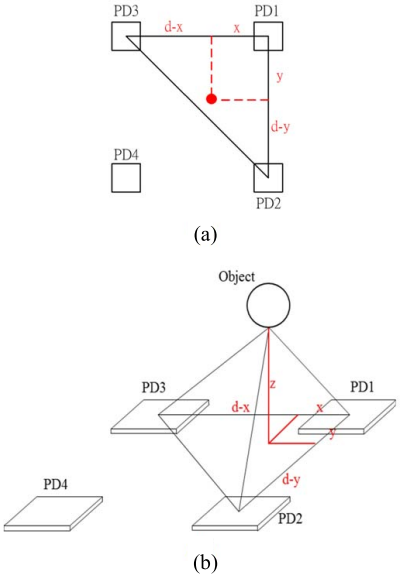

Fig. 3. The schematic of the object and the PD array. (a) Top view; (b) 3-D view.

simultaneously, one is able to find the 3D coordinates of the object to detect. With complex computation conducted, the solutions for the 3D object are

$$x = \frac{d}{2} - \frac{R_3 - R_1}{d} z = \frac{d}{2} - \frac{\sqrt{\beta}}{2}\left(\frac{1}{\sqrt{V_3}} - \frac{1}{\sqrt{V_1}}\right)\frac{z}{d}, \quad (11)$$

$$y = \frac{d}{2} - \frac{R_2 - R_1}{d} z = \frac{d}{2} - \frac{\sqrt{\beta}}{2}\left(\frac{1}{\sqrt{V_2}} - \frac{1}{\sqrt{V_1}}\right)\frac{z}{d}, \quad (12)$$

The calculation of (11) and (12) above, and (13) shown at the bottom of the page is carried out by the combined codes of MATLAB and LABVIEW. In the codes, β is estimated by optics, PD properties and circuit parameters, and/or calibrated based on prior experiment data.

III. Sensing Circuit

A. The Conventional 3T-APS Circuit

The conventional active pixel sensor is so-called 3T-APS, standing for 3 transistors (3T) and active pixel sensor (APS). The schematic is shown in Fig. 4. It consists of three MOSFETs and one photo detector. This 3T-APS needs a RESET clock for controlling $M1$ switch. When $M1$ turns on, the parasitic capacitance of the photo detector is charged from bias voltage. When $M1$ turns off, the parasitic capacitance of the photo detector is discharged by the photocurrent which is generated by the photo detector. On the other hand, $M2$ plays the role as a unit gain buffer for isolating the photo detector from the external noises. Finally, $M3$ does the role as a switch for selecting the pixels. With this topology, noise reduction

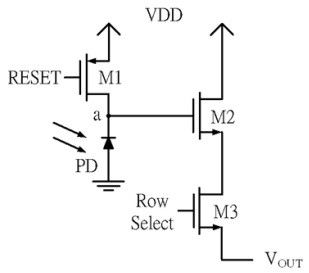

Fig. 4. The schematic of the 3T active pixel sensor.

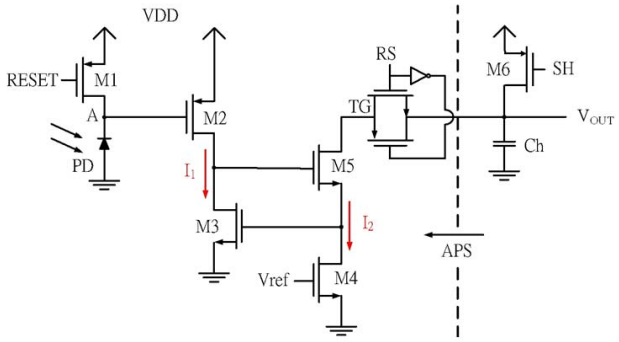

Fig. 5. The new active pixel circuit.

and high output linearity is achievable, while suffering the only disadvantage that the output voltage range is limited by $M2$ overdrive, noting that the maximum output voltage is bias voltage – V_{DS} ($M2$). In other words, the drawback of 3T-APS is a limited output range, thus the maximum output not being up to bias voltage. The output range and resolution of this conventional 3T-APS is intended to be improved by this study, as stated in the following subsection.

B. The New Active Pixel Sensor Circuit

A new active pixel sensor circuit is designed and shown in Fig. 5. The photodiode which plays the role of a photo detector is operated with reverse bias. The photodiode is charged and discharged through $M1$. $M2$ acts as a buffer for isolating the photodiode from the external noise. $M3 \sim M5$ comprise an adjustable current mirror. *TG* is a transmission gate for choosing which pixel should be read. The output range of this new APS is larger than the afore-mentioned conventional 3T-APS, rendering a better output resolution. The operation of the new APS is elaborated below as a two-stage one. *TG* is constantly turned on for only one pixel, therefore the voltage at *RS* is 3.3 V.

1) Reset Mode: *Reset* and *SH* are turned to low-states (0V). $M1$ and $M2$ are turned on. The parasitic capacitance of the photodiode and C_h are charged. The voltage at node A is raised to the bias voltage.

$$z = \frac{\left(\frac{1}{2}\sqrt{\frac{\beta}{V_2}} + \frac{1}{2}\sqrt{\frac{\beta}{V_3}}\right) \pm \sqrt{-\frac{\beta}{4V_3} - \frac{\beta}{4V_2} - \frac{\beta}{V_1} + \frac{\beta}{\sqrt{V_1 V_3}} + \frac{\beta}{\sqrt{V_1 V_2}} + \frac{\beta}{2\sqrt{V_2 V_3}} - 2d^2}}{2\frac{\frac{\beta}{4V_3} + \frac{\beta}{4V_2} + \frac{\beta}{2V_1} - \frac{\beta}{2\sqrt{V_1 V_3}} - \frac{\beta}{2\sqrt{V_1 V_2}} + d^2}{d^2}}. \quad (13)$$

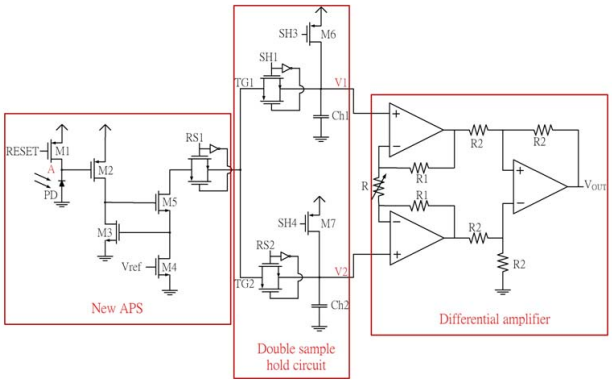

Fig. 6. The schematic of the designed IC.

2) Read Mode: *Reset* and *SH* are turned to high state (bias voltage). $M1$ and $M2$ are turned off. With the photocurrent starting to discharge the parasitic capacitance of the photodiode, the voltage at node A is decreasing. The speed of the voltage decrease at A is determined by the received intensity of the photodiode.

C. The 3D Optical Proximity Sensing Circuit

With an object closing the module, the light from LEDs emits to the object and then reflects to the PD. The photo detector receives both the reflected light and the background light when the LEDs are on. The background light should change with the environment. In order to have the system function as well as in different lighting environments, the background light needs to be eliminated. The previous readout circuit is extended to eliminate the effects of the different environments.

The process of eliminating the background light is completed with a specially-designed circuit as shown in Fig. 6. The circuit includes three parts. The first part is the APS circuit for driving a photodiode. The second part is the double sample hold circuit. With the LED on and off, the output voltages of APS are stored in the double-sample-hold circuit separately. The final part of circuit is a differential amplifier, which subtracts two voltages from two sample-and-hold circuit outputs. With LEDs on, the voltage is stored by the sample-and-hold circuits with the photo detector receiving the reflected light and background light. As the LED is turned off, the voltage stored by sample-and-hold circuit contains those from the photo detector receiving the background light only. After the subtraction via the differential amplifiers, the output voltage reflects the intensity level of the reflected light. The multiple voltage outputs can be analyzed to calculate the distance from an object to the sensor module plane; i.e., z coordinates and x, y positions without considering the environment light.

Based on the aboves, the IC designed in this study includes the new designed APS and the circuit for eliminating the background light, as shown in Fig. 6. The operation process is explained below.

1) Reset Mode in $T1$. LED is turned on. $M1$, $M6$ and *TG1* are turned on. The parasitic capacitance of the photodiode is charged. The voltage at node A and V_1 are raised to the bias voltage.

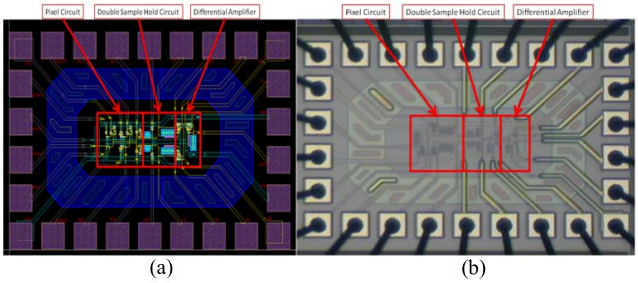

(a) (b)

Fig. 7. (a) The layout of the designed IC. (b) The micro-photo of the fabricated IC.

2) Read Mode in $T1$. LED is turned on. $M1$, $M6$ are turned off. *TG1* is turned on. The voltage at node A is reduced since the photodiode receives both the reflected light and background light. The current mirror composed of $M3 \sim M5$ copies the current from $M2$ proportionally. C_{h1} is next discharged, while the *TG1* turned off and V_1 samples the voltage.
3) Reset Mode in $T2$. LED is turned off. $M1$, $M7$ and *TG2* are turned on. The parasitic capacitance of the photodiode is charged. The voltage at node A and V_2 are raised to the bias voltage.
4) Read Mode in $T2$. LED is turned off. $M1$, $M7$ are turned off. *TG2* is turn-on. The voltage at node A is in decrease since the photodiode receives the background light. The current mirror composed of $M3 \sim M5$ then copies the current from $M2$ proportionally. C_{h2} is then discharged, while *TG2* is turned off and V_2 sampled the voltage.
5) With the very rear-end the differential amplifier, V_{OUT} can be expressed as

$$V_{OUT} = (1 + \frac{2R_1}{R})(V_2 - V_1). \tag{14}$$

Then the relationship between the photocurrent and V_{OUT} is

$$V_{OUT} = (1 + \frac{2R_1}{R})\frac{t}{C_m} I_R. \tag{15}$$

In Eqs. (14), (15), I_R is the photocurrent generated by the reflected light. C_{in} is the equivalent capacitance at the negative end of the photodiode. t is the discharge time of photodiode. V_1 voltage contains the effect of background and reflects light, while V_2 does only the effect of the background light. Having operated the differential amplifier effectively, two voltages from two sample-and-hold circuit outputs are subtracted by proper timing switchings. The output voltage thus corresponds to the reflected light, i.e., V_{OUT} indicates only the effect of the light reflected from the object.

IV. Measurement

The proposed circuit and PDs are realized by the TSMC 0.35um Mixed Signal 2P4M process. The supply voltage is 3.3 V. The fabricated chip area of IC is 0.8×1.22 mm^2. The layout plot and the photo of the readout chip are shown in Fig. 7. The designed IC has 28 pins. On the other hand, the PD chips are measured with a confirmed sensitivity of 0.775 micro- photocurrent (μA) per radiant flux of 10-5 Watts.

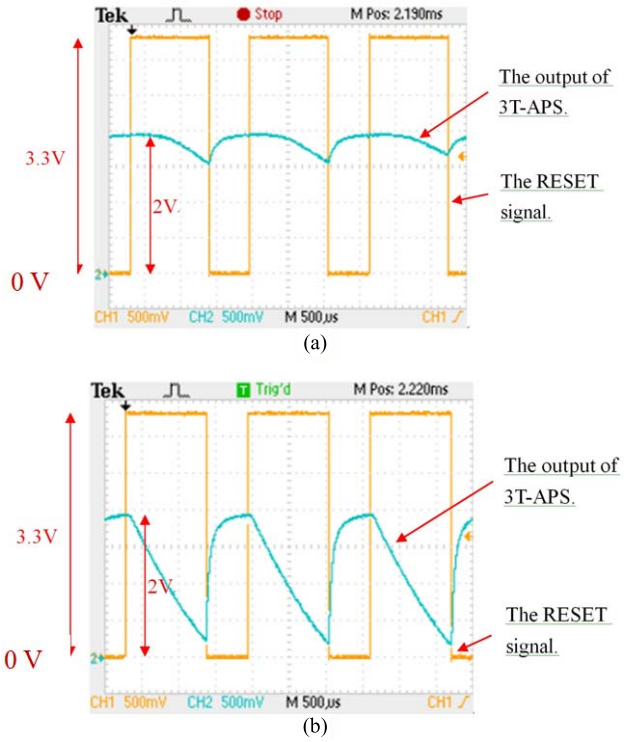

Fig. 8. Chip measurements of the conventional 3T APS with (a) weak light and (b) strong light.

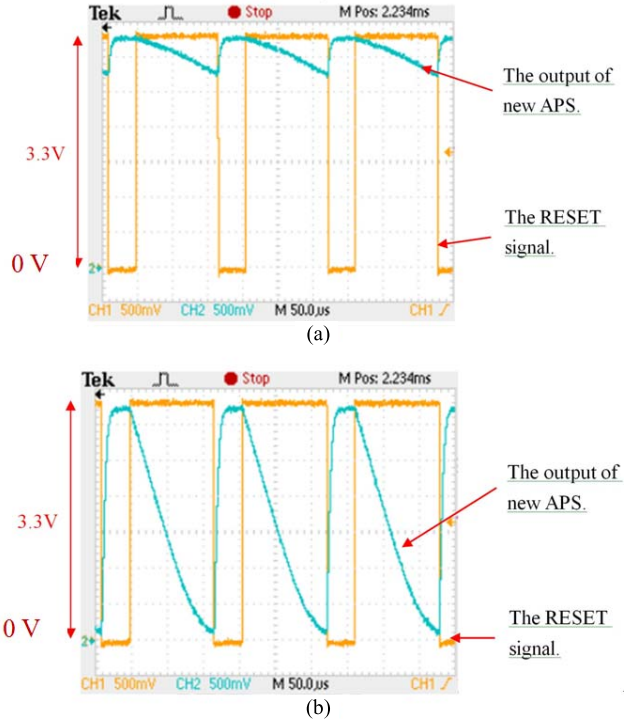

Fig. 9. Chip measurements of the new APS with (a) weak light and (b) strong light.

The LEDs adopted are those modeled HIRB1b-48C with individual emission luminous intensity of 12 mw/sr as driven by a nominal current of 10 μA. The control signals are generated by an FPGA board (Xilinx XC3S500E Spartan-3E FPGA). In this study, the new APS and the CMOS-processed PDs are implemented in the designed IC.

A. Active Pixel Sensor Circuit

The measurements for evaluating the performance of the fabricated chip circuit for the conventional 3T-APS and the new APS are shown in Figs. 8 and 9. In order to simulate the environment with strong light, the LEDs other than those on the sensing panel emits the light to the PDs directly, while another case for the environment with weak light is also considered, where the sensor is tested in the dark room. In Fig. 8, the maximum output of conventional 3T-APS is about 2V, while the minimum output is 0 V. It is clear that the maximum output of the conventional APS is limited. The output range from 2V to 3.3V is wasted. On the other hand, the new APS has a larger output range as shown in Fig. 9. The maximum output can reach 3.3 V, while the minimum output is 0V. With the experiment accomplished, the new APS is actually shown to own a larger output range then the conventional 3T-APS.

B. Sensor Panel System

Measurements on the system IC is conducted next. The system for measurement is composed of the PD/LED array, FPGA board and designed IC. The distance from PDs to the object is changed from 0.5 cm to 3.5 cm for testing the sensing

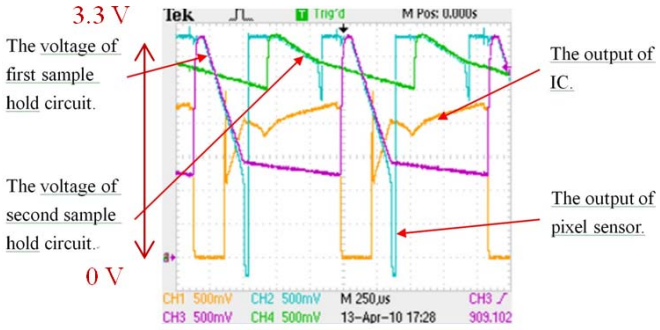

Fig. 10. Measurements of the readout IC with the object distance 0.5 cm.

panel. The experiment results are shown in Figs. 10 and 11. The blue curve contains the outputs of an APS. The green and purple curves are the output signals of the double sample and hold circuit. The orange curve is the output of the entire IC. It is evidence from Figs. 10 and 11 that the outputs of both sample and hold function properly despite slight continuous drop on the voltage across the output capacitances, which is due to inevitable current leakage of the capacitors. On the other hand, based on the comparison between two figures, the outputs of the first sample and hole in greens are the same while the outputs of the second in purple changes. This is due to the fact that the first sample-and-hold receives only ambient light while the second does also reflected light. Furthermore, the output of the entire circuit in orange curves decreases as the object to detect positioned away from the sensing panel. The relation between the output signal and object distance is summarized by Fig. 12, where a one-to-one

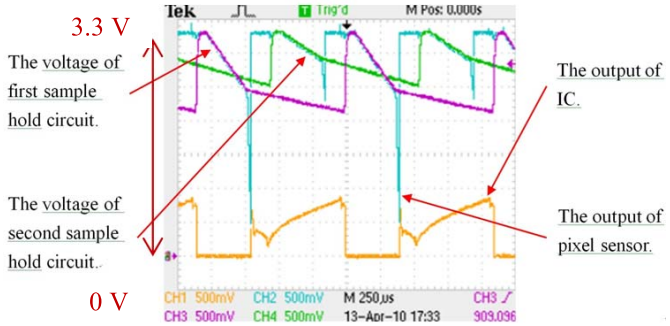

Fig. 11. Measurement of the readout IC with the object distance 3.5 cm.

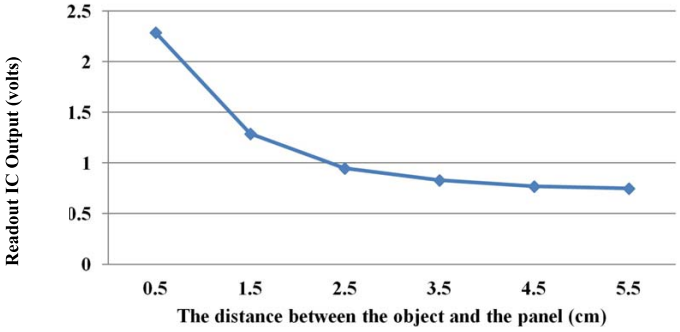

Fig. 12. The measured outputs of the fabricated IC versus the distance between the object and the sensor panel.

correspondence between the object distance and the circuit output voltage is available for sensing the 3D coordinates of the object interested.

It should be noted that the adopted sample-and-hold circuitry in Fig. 6 is in low noise, since it is by nature an integrating circuit, as evidenced by low-noise signals in Figs. 8–11. In addition, the basic technique of "moving averaging" and low-pass filters are also applied in the final stage of signal processing the Labview program to reduce noise. Finally, the calibration establishes successfully the true relation between the object 3D position and PD outputs, in which case, supposedly, the effects of offsets/nonlinearities and those by post-processing averaging are minimized. In a short conclusion, the noise does not play a significant factor in designing and validating the proposed sensor system.

V. Experimental Results

A real-time 3D object position sensing panel is realized by this study. Fig. 13 demonstrates the experimental configuration for study on the sensing panel. The photo in Fig. 14(a) shows an example of a flexible panel. Note that in this study experiments are conducted with the panel set flat for pioneer performance testing. On the other hand, a user GUI interface installed in a computer is established for monitoring real-time object motion. The object to detect is a styrofoam ball with a radius of 1.5 cm. The PDs and LEDs array comprise the front-end sensor panel. The photo showing the experiment conduction is given in Fig. 14(b).

The signals from the PD/LED array are received by the designed IC. Having conducted signal processing by an

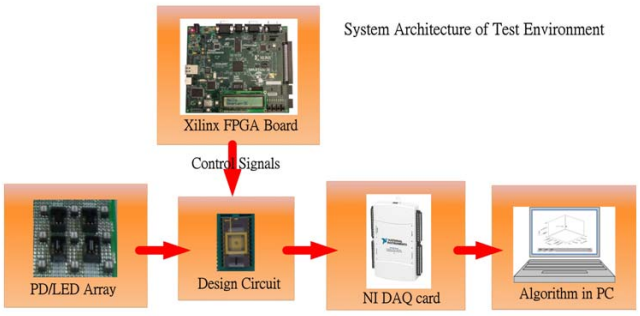

Fig. 13. The configuration of the test system.

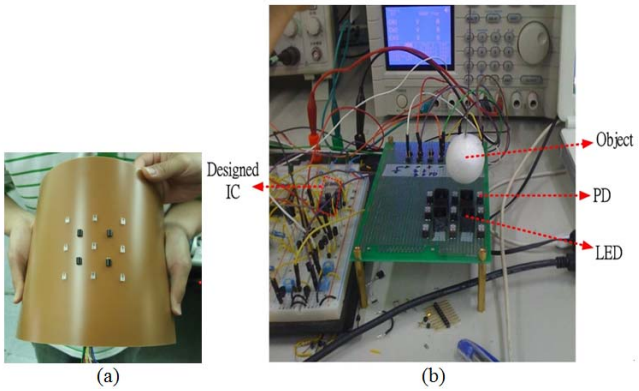

Fig. 14. (a) An example of the sensor panel. (b) The experimental setup.

TABLE I
Errors in Distance Between Realistic Coordinates and Measured Counterparts With the Test Object at the Distance of 3 cm

Realistic Coordinates (cm)	Predicted Results (cm)	Errors in Distance (cm)
(0 , 0 , 3)	(0.149 , 0.252 , 3.133)	0.103
(2 , 0 , 3)	(1.901 , 0.212 , 3.231)	0.302
(2 , 2 , 3)	(1.928 , 1.948 , 3.080)	0.12
(0 , 2 , 3)	(-0.033 , 1.901 , 2.978)	0.107
(1 , 1 , 3)	(0.899 , 1.144 , 3.182)	0.153

TABLE II
Errors in Distance Between Realistic Coordinates and Measured Counterparts With the Test Object at the Distance of 4 cm

Realistic Coordinates (cm)	Predicted Results (cm)	Errors in Distance (cm)
(0 , 0 , 4)	(0.148 , 0.255 , 4.04)	0.298
(2 , 0 , 4)	(1.869 , 0.254 , 4.198)	0.322
(2 , 2 , 4)	(1.887 , 1.869 , 4.09)	0.195
(0 , 2 , 4)	(-0.199 , 1.744 , 3.84)	0.362
(1 , 1 , 4)	(0.819 , 0.97 , 4.034)	0.187

afore-designed IC, the background light effects are eliminated. The output signals of IC depend only on the reflected light intensity. The output signal of the IC is read by a DAQ card (NI USB-6212), and then the calculation based on the algorithm developed in section II is preformed to find out the

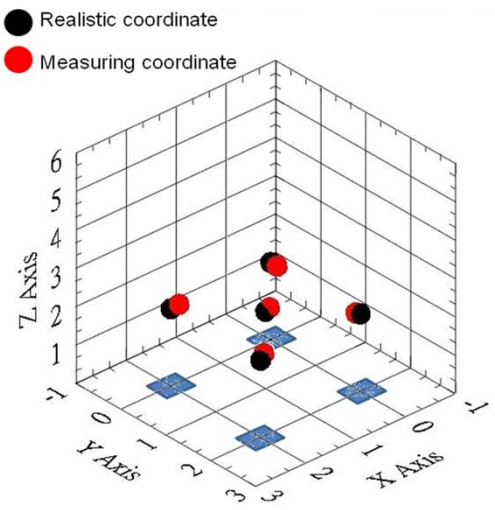

Fig. 15. The predicted and realistic 3D coordinates with 3 cm between the sensor panel and the object to detect.

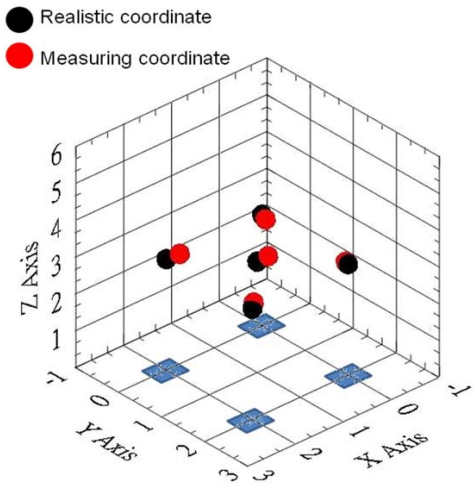

Fig. 16. The predicted and realistic 3D coordinates with 4 cm between the sensor panel and the object to detect.

3D coordinates of the object to detect, which are carried out by a LABVIEW (LABVIEW 8.6) code. The calculation and the display for the near-real-time 3D positions and motions of the moving object are accomplished by a pre-designed LABVIEW program, as shown in Figs. 15 and 16. Future effort will be dedicated to realize the computation and display via newly-designed digital chips, aiming for no-delays sensed by users.

Figs. 15 and 16 are the test results of predicting the object coordinates, which correspond to the object distances of 3 and 4 cm from the sensor module. The results of error analysis are also shown in Figs. 15 and 16 and Tables I and II in numbers. The black points are the realistic positions of the object. The red points are the calculated results of the system. The blue squares at the bottom are the photo detectors. As seen from Figs. 15 and 16 and the results in Tables I and II, the predicted 3D coordinates are close to those realistic values despite the error grows as the object continues to move away from the sensing panel. The errors are mostly resulted from inadequate accuracy of the PD/LED array, which mainly due to sparsity of PDs and the non-uniformity of opto-electric properties across different PDs. Besides, there are other types of errors in system, like the noise in the readout circuit. According to the test results, the calculated 3D coordinates of the object are particularly less accurate between two PDs. One of the methods to solve problem is that the PD/LED array is to be made with much more consistent opto-electrical properties of devices and more densely distributed PDs and LEDs in larger numbers. Another means is to adjust the gains of different amplifier in the readout IC to balance four PDs outputs.

VI. Conclusion

This study proposes a new 3D optical proximity sensing panel for sensing a single object. Its readout circuit and computation algorithm have been successfully built for satisfactory accuracy. This 3D sensing panel is composed of PD/LED arrays, FPGA, designed IC and a LABVIEW program. In this system, the LED emits the light to the object, and then the light reflected from the object is sensed by the PDs. The PDs in the array are fabricated by the TSMC CMOS 0.35um Mixed-Signal 2P4M process which is available for photodiodes. Each PD in the array is equipped with a newly-designed front-end readout circuit, forming a new so-called active pixel sensor (APS). As compared to the conventional 3T-APS, this new APS and readout has been proven advantageous in larger output ranges and higher resolutions.

Following the APSes are the designed/fabricated sample and hold circuits and differential amplifiers, which are capable of eliminating background noise that is partly induced by environmental light. PD/APS outputs are next fed to a data acquisition module and then a computer for carrying out the computation based on optical photometry to retro-calculate the 3D coordinates of the object. Also, the reflected light signal is received by a DAQ card and sent to a LABVIEW code for displaying real-time object motions. Predicted 3D coordinates of the object are collected, followed by the associated error analysis. It has been well proven that the designed 3D optical proximity sensing panel is effective in predicting the 3D coordinates of an object in front of the sensing panel with satisfactory accuracy. In the future, effort will be dedicated to design and fabricate a mixed-signal ASIC chip to include both front-end analog circuits for signal acquisition and digital circuits for algorithm computations, thus towards a complete small-sized system-on-chip for readout. Also, the possibilities of "multi-touch," i.e., detecting multiple objects, will be explored.

References

[1] Z. Chen and R. C. Luo, "Design and implementation of capacitive proximity sensor using microelectromechanical systems technology," *IEEE Trans. Ind. Electron.*, vol. 45, no. 6, pp. 886–894, Dec. 1998.

[2] S. I. Cho, S. I. Lim, K. H. Baek, and S. Kim, "Capacitive proximity sensor with negative capacitance generation technique," *Electron. Lett.*, vol. 48, no. 22, pp. 1409–1411, Oct. 2012.

[3] F. Lebahn, H. Krüger, and H. Ewald, "Investigations to the side-metal-effect of inductive proximity sensors under usage of 3D time-harmonic eddy-current field solver," in *Proc. 4th ICMSAO*, Apr. 2011, pp. 1–3.

[4] P. M. Novotny and N. J. Ferrier, "Using infrared sensors and the Phong illumination model to measure distance," in *Proc. IEEE Int. Conf. Robot. Autom.*, May 1999, pp. 1644–1649.

[5] A. Tar, M. Koller, and G. Cserey, "3D geometry reconstruction using large infrared proximity array for robotic applications," in *Proc. IEEE ICM*, Apr. 2009, pp. 1–6.
[6] D. Um and W. N. P. Hung, "A novel infrared proximity array sensor for 3D visual sensing: Modeling and applications," in *Proc. IEEE Conf. Robot., Autom. Mechatron.*, Jun. 2006, pp. 1–6.
[7] K. Hsiao, P. Nangeroni, M. Huber, A. Saxena, and A. Y. Ng, "Reactive grasping using optical proximity sensors," in *Proc. IEEE Int. Conf. Robot. Autom.*, May 2009, pp. 2098–2105.
[8] A. Buchan, J. Bachrach, and R. S. Fearing, "Towards a minimal architecture for a printable, modular, and robust sensing skin," in *Proc. IEEE/RSJ Int. Conf. Intell. Robots Syst.*, Oct. 2012, pp. 33–38.
[9] D. Ryu, D. Um, P. Tanofsky, D.-H. Koh, Y.-S. Ryu, and S. Kang, "T-less : A novel touchless human-machine interface based on infrared proximity sensing," in *Proc. IEEE Int. Intell. Robots Syst. Conf.*, Oct. 2010, pp. 5220–5225.
[10] H. Ting, C. Bisdikian, L. Kaplan, W. Wei, and D. Towsley, "Multi-target tracking using proximity sensors," in *Proc. Military Commun. Conf.*, Nov. 2010, pp. 1777–1782.
[11] S. Tsuji, "A tactile and proximity sensor by optical and electrical measurement," in *Proc. IEEE Sensors Conf.*, Oct. 2012, pp. 1–4.
[12] N. Faramarzpour, M. J. Deen, S. Shirani, Q. Fang, L. W.-C. Liu, F. de Souza Campos, *et al.*, "CMOS-based active pixel for low-light-level detection: Analysis and measurements," *IEEE Trans. Electron Devices*, vol. 54, no. 12, pp. 3229–3237, Dec. 2007.
[13] S. Hanson, Z. Foo, D. Blaauw, and D. Sylvester, "A 0.5 V sub-microwatt CMOS image sensor with pulse-width modulation readout," *IEEE J. Solid-State Circuits*, vol. 45, no. 4, pp. 759–767, Apr. 2010.
[14] S. Mendis, S. E. Kemeny, and E. R. Fossum, "CMOS active pixel image sensor," *IEEE Trans. Electron Devices*, vol. 41, no. 3, pp. 452–453, Mar. 1994.
[15] M. Maolinbay, Y. El-Mohri, L. E. Antonuk, K.-W. Jee, S. Nassif, X. Rong, *et al.*, "Additive noise properties of active matrix flat panel imagers," *Med. Phys.*, vol. 27, no. 8, pp. 1841–1854, 2000.
[16] I. Ashdown, *Radiosity: A Programmer's Perspective*. Singapore: Heart Consultants LTD., 2002.

Sheng-Chieh Huang was born in Chunghua, Taiwan, in 1967. He is currently an Assistant Professor with the Department of Electrical and Computer Engineering, National Chiao Tung University, Hsinchu, Taiwan.

Wei-Hsuan Hsu received the M.S. degree from the National Chiao Tung University, Taiwan, in 2010. His current research interests include optical proximity sensor and integral circuit design. He was with Wistron from 2011 to 2013.

Paul C.-P. Chao received the M.S. and Ph.D. degrees from Michigan State University, USA. He was with the CAE Department, Chrysler Corporation, Auburn Hill, Detroit, MI, USA, for two years. He is currently a Faculty Member of the Electrical Engineering Department, National Chiao Tung University (NCTU), Taiwan. Prof. Chao was the recipient of the Arch T. Colwell Merit Best Paper Award from the Society of Automotive Engineering, Detroit, MI, USA, in 1999, the Long-Wen Tsai Best Paper Award from the National Society of Machine Theory and Mechanism, Taiwan, in 2004, the Best Paper Award from the National Society of Engineers, Taiwan, in 2005, the CYCU Innovative Research Award from 2002 to 2004, the AUO Award in 2006, the Acer Long-Term 2nd-Prize Award in 2007, the NCTU EEC Outstanding Research Award from 2007 to 2009, the Best Paper Award from the Symposium on Nano-Device Technology in 2009, and the Best Paper Award from the 20th Annual IEEE/ASME Conference on Information Storage and Processing Systems (ISPS) in 2010. He was the Associate Provost with NCTU, the Secretary of the IEEE Taipei Section, from 2009 to 2010, and currently the Founding Chair of the local chapter for the IEEE Sensor Council and an AdCom Member of the IEEE Sensors Council. He is the Associate Editor of three well-known SCI-index journals, the IEEE SENSORS JOURNAL, the *ASME Journal of Vibration and Acoustics*, and the *Journal of Circuit, System, and Computer*. In recent years, his current research interests include interface analog circuit design for optical devices/systems, micromechatronics, control technology, microsensors, and microactuators.

Che Hung Tsai received the B.S. and M.S. degrees in electrical engineering from I-Shou University, Taiwan, in 2006 and 2008, respectively. He is currently pursuing the Ph.D. degree with National Chiao Tung University, Taiwan. His current research interests include linear control, integral circuit design, and photonic crystal.